JACS
JOURNAL OF THE AMERICAN CHEMICAL SOCIETY
Article
pubs.acs.org/JACS

$Pd_6O_4^+$: An Oxidation Resistant yet Highly Catalytically Active Nano-oxide Cluster

Samdra M. Lang,[†] Irene Fleischer,[†] Thorsten M. Bernhardt,*[,†] Robert N. Barnett,[‡] and Uzi Landman*[,‡]

[†]Institute of Surface Chemistry and Catalysis, University of Ulm, Albert-Einstein-Allee 47, 89069 Ulm, Germany
[‡]School of Physics, Georgia Institute of Technology, Atlanta, Georgia 30332-0430, United States

Supporting Information

ABSTRACT: The palladium oxide cluster $Pd_6O_4^+$ is formed as the sole product upon reaction of a bare palladium cluster Pd_6^+ with molecular oxygen in an octopole ion trap under multicollision conditions. This oxide cluster is found to be resistant to further oxidation over a large temperature range, and further O_2 molecules merely physisorb on it at cryogenic temperatures. The particular stability of $Pd_6O_4^+$ is confirmed by the observation that the reaction of Pd_7^+ with O_2 leads to fragmentation resulting in the formation of $Pd_6O_4^+$. However, in an oxygen-rich O_2/CO mixture, $Pd_6O_4^+$ is identified as the catalytically active species that effectively facilitates the low-temperature oxidation of CO. Gas-phase reaction kinetics measurements in conjunction with first-principles calculations provide detailed molecular level insight into the nano-oxide cluster chemistry and are able to reveal the full catalytic combustion reaction cycle.

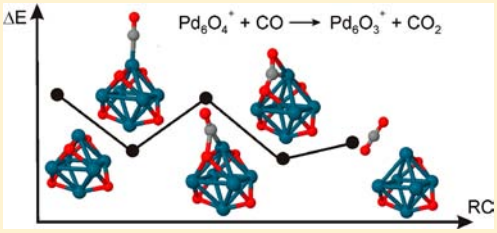

1. INTRODUCTION

Nanometal oxides are an important class of heterogeneous catalysts for various industrial processes.[1,2] Several factors are considered as governing the catalytic activity and selectivity of these catalytic materials, including particle size, shape, composition, and, in particular, the chemical nature of the active oxygen species. Consequently, correlations between the oxidation states and catalytic activity are a fundamental topic of investigations pertaining to catalytic activity in general and of oxides in particular.[2]

Palladium is the most known and often used catalyst for CO combustion, particularly because of its employment in three-way catalysts in automotive combustion systems.[3] Research pertaining to the oxidation of CO on extended palladium single crystal surfaces has been pioneered more than three decades ago, and details of the reaction mechanisms, energetics, and poisoning effects have been elucidated.[4]

More recently, experimental and theoretical research focused on the chemical and catalytic properties of oxide supported nanoscale Pd particles, aiming at the design of new efficient low-temperature oxidation catalysts and at understanding the particle- size-dependent oxide modifications. Pd nanoparticles (containing hundreds, or thousands, of atoms) were found to form diverse oxygen species, including interfacial, surface, subsurface, and bulk oxygen or PdO-like oxide shells, with the particular species formed depending on the applied reaction conditions and on particle dimensions.[5,6] However, current information about the role of different oxygen species in the catalytic behavior of the particles is still incomplete. CO oxidation experiments on Fe_3O_4 supported Pd nanoparticles (average diameter of 7 nm) revealed the reversible formation of a thin Pd oxide layer at the metal/support interface, which serves as an oxygen reservoir, while oxygen chemisorbed on the metallic Pd nanoparticle was identified to be directly involved in the CO oxidation reaction.[6] This finding is in agreement with a systematic study on different Pd−O species revealing decreasing CO oxidation activity with increasing oxidation state and identifying chemisorbed oxygen O(ad) on metallic Pd(111) as the most reactive oxygen species.[7]

On small magnesia (MgO)-supported palladium clusters, an unexpected low dissociation barrier of adsorbed O_2 was found theoretically.[8−10] In particular, for the case of a surface-supported pyramidal palladium cluster, Pd_{30}/MgO(100), the dissociation barriers for multiple adsorbed oxygen molecules were found to be exceedingly small (<0.1 eV) at adsorption sites that are at, or near, the interface of the cluster with the MgO surface. On the other hand, dissociation of O_2 molecules at other sites on the supported cluster entails prohibitively large barriers, resulting in a self-limiting partial (interfacial) oxidation of the metal cluster.[9] This behavior correlates with activation (to a peroxo state) of the interfacially adsorbed oxygen molecules via fractional occupation of the antibonding ($2\pi^*$) molecular orbitals by excess electronic charge localized at the magnesia-to-Pd cluster interface. The partially oxidized Pd clusters were shown to act as Mars−van Krevelen[11] oxygen reservoirs in the CO-catalyzed oxidation reaction, correlating with isotope-labeling temperature programmed reaction (TPR) experiments (see refs 9 and 10 for a smaller surface-supported Pd_{13} cluster).

In the context of the reactivity of small gas-phase clusters, we note that recently the importance of oxygen radical centers in the oxidation of CO by preoxidized free PdO_2^+ and PdO_3^+ clusters has been demonstrated utilizing guided-ion-beam mass

Received: August 17, 2012
Published: December 14, 2012

spectrometry and theoretical calculations.[12] Furthermore, a reactivity study performed in an octopole ion trap revealed fast formation and elimination of CO_2 by exposure of preoxidized palladium clusters, Pd_xO^+ (x = 3−5) and $Pd_xO_2^+$ (x = 4−6), to CO. In contrast, the oxidation of CO on Pd_2O^+, Pd_6O^+, and Pd_7O^+ was found to be hampered, indicating that enhanced activation barriers may be involved in the CO oxidation and/or the occurrence of a CO_2 elimination process.[13] Additionally, in a theoretical investigation of the interaction between $Pd_4O_y^{+/0/-}$ (y = 1, 2) and CO, cationic clusters were found to show enhanced catalytic activity as compared to anionic and neutral ones, due to reduced CO and CO_2 binding energies.[14]

In an effort directed at identification of the catalytically active species, and to gain further insight into the corresponding reaction mechanisms, the oxidation behavior and catalytic properties (in the CO combustion reaction) of a series of small cationic palladium clusters, Pd_x^+ (x = 2−7), were investigated systematically by us via gas-phase ion trap mass spectrometry and first-principles density functional theory (DFT) simulations. Among all of the investigated clusters, the cation hexamer, Pd_6^+, exhibited exceptional reactive properties with respect to both oxidation behavior and catalytic CO combustion. Therefore, in this Article, we focus exclusively on a molecular level investigation of the formation of $Pd_6O_4^+$ and its catalytic activity, while details for the other clusters, Pd_x^+ with $2 \le x \le 7$, may be found in forthcoming contributions.

2. METHODS

2.1. Experimental Setup and Data Evaluation. The gas-phase reactions of the palladium hexamer Pd_6^+ have been studied in a radio frequency (rf) octopole ion trap embedded into a low-energy ion beam assembly of quadrupole ion guides and mass spectrometers. The general experimental layout has been described in detail elsewhere[15] and will only be outlined briefly here.

The palladium cations Pd_6^+ are generated by simultaneously sputtering four metal targets with Xe ions produced by a CORDIS (cold reflex discharge ion source).[16] The formed cluster ion beam is steered into a first helium filled quadrupole ion guide to collimate and thermalize the hot clusters. Subsequently, cluster ions of the desired size are selected from the beam by means of a first mass-selecting quadrupole filter and are transferred via a second quadrupole ion guide into the home-built octopole ion trap. The ion trap is prefilled with about 1 Pa helium buffer gas and a small but variable fraction of O_2 or a mixture of O_2 and CO. Furthermore, the ion trap is attached to a closed cycle helium cryostat in combination with a resistive heater that allows for temperature adjustment in the range between 20 and 300 K. Thermal equilibration of the clusters is achieved within a few milliseconds under our experimental conditions,[15] while the clusters are stored for considerably longer time, typically between 0.1 s and several seconds.

After reaction of the clusters in the ion trap for a chosen time (reaction time t_R), all ions, intermediates, and final products are extracted, and the ion distribution is analyzed in a second quadrupole mass filter. Kinetic data are obtained by recording the intensity of all ion signals as a function of the reaction time. The normalized kinetic traces are then evaluated by fitting the integrated rate equations of potential reaction mechanisms to the experimental data utilizing the software package "Detmech".[17] This leads to the determination of the simplest reaction mechanism that best fits the experimental data as well as the corresponding rate constant k.

Because the total pressure in the ion trap amounts to about 1 Pa, which means that the experiment is operated in the kinetic low pressure regime, the details of each association reaction step, for example:

$$Pd_6^+ + O_2 \rightarrow Pd_6O_2^+, \quad k \tag{1}$$

can be described by the Lindemann energy transfer model for association reactions:[18,19]

$$Pd_6^+ + O_2 \rightleftarrows (Pd_6O_2^+)^*, \quad k_a, k_d \tag{2a}$$

$$(Pd_6O_2^+)^* + He \rightarrow Pd_6O_2^+ + He^*, \quad k_s \tag{2b}$$

According to this model, the reaction of Pd_6^+ with O_2 yields the energized complex $(Pd_6O_2^+)^*$ (association rate constant k_a). This complex can either decompose back to the reactants (decomposition rate constant k_d) or be stabilized via collision with a helium buffer gas atom (stabilization rate constant k_s).

Consequently, the reaction depends on the helium buffer gas pressure and becomes of third order. However, the oxygen [O_2] and helium buffer gas [He] concentrations in the ion trap are orders of magnitude larger than the cluster ion concentration, and a steady flow of these reactants is ensured. This permits the postulation of pseudofirst-order kinetics with the pseudofirst-order rate constant:

$$k = k^{(3)}[He][O_2] \tag{3}$$

containing the termolecular rate constant $k^{(3)}$ as well as the buffer gas and oxygen concentration.

2.2. Theoretical Methods. The theoretical explorations of the atomic arrangements and electronic structures of Pd_x^+ clusters and their complexes with oxygen were performed with the use of first-principles density functional theory (DFT) calculations. In particular, we employed the Born−Oppenheimer (BO)-spin density functional (SDF)-molecular dynamics (MD) method, BO-SDF-MD,[20] with norm-conserving soft (scalar relativistic for Pd) pseudopotentials[21] and the generalized gradient approximation (GGA)[22] for electronic exchange and correlations. In these calculations, we have used a plane-wave basis with a kinetic energy cutoff E_c = 110 Ry, which yields convergence. This corresponds to a real-space grid spacing of 0.3 a_0; the real-space grid spacing for the density was 0.1 a_0 corresponding to E_c = 987 Ry. In the construction of the Pd pseudopotentials, the valence electrons, $4s^2$, $4p^6$, and $4d^{10}$, were characterized by core radii r_c = 0.85 a_0, 0.90 a_0, and 1.15 a_0, respectively, with the s orbital treated as local; a_0 is the Bohr radius. The BO-SDF-MD method is particularly suitable for investigations of charged systems because it does not employ a supercell (i.e., no periodic replication of the ionic system is used). In all of the calculations, the dependence on spin multiplicity has been checked, and the results that we report correspond to the spin multiplicities with the lowest energies; for early prediction of the magnetic properties of palladium clusters, see ref 23. Structural optimizations were performed using a conjugate-gradient-like method.

In the first-principles calculations of the reaction profiles (pathways, see Figure 4 and the Supporting Information), a reaction coordinate was judiciously chosen; typically, the reaction coordinate consists of the distance between two atoms of the reactant molecules (for example, an O atom of an adsorbed oxygen molecule and the C atom of a reacting CO molecule). For each value of the reaction coordinate, the total energy of the system was optimized through unconstrained relaxation of all of the other degrees of freedom of the system (reactants, other adsorbents, and Pd cluster atoms). The reaction profiles (reaction paths) were obtained via repeating such calculations for various values of the chosen reaction coordinate. These calculations yield results that are the same as, or close to, those obtained by other methods, for example, the nudged elastic band and variants thereof; see the discussion on pp 89 and 90 in ref 24.

3. RESULTS AND DISCUSSION

3.1. Tetroxide Formation. Figure 1a displays a representative ion mass distribution obtained after reaction of the bare palladium cluster Pd_6^+ with molecular oxygen for 0.1 s at 300 K. It shows fast adsorption of two oxygen molecules and formation of a single reaction product $Pd_6O_4^+$. A similar reaction product has also been observed for negatively charged Pd_6^- previously, although no details on the intensity and stability of this product were given.[25] To quantify the

dx.doi.org/10.1021/ja308189w | J. Am. Chem. Soc. 2012, 134, 20654−20659

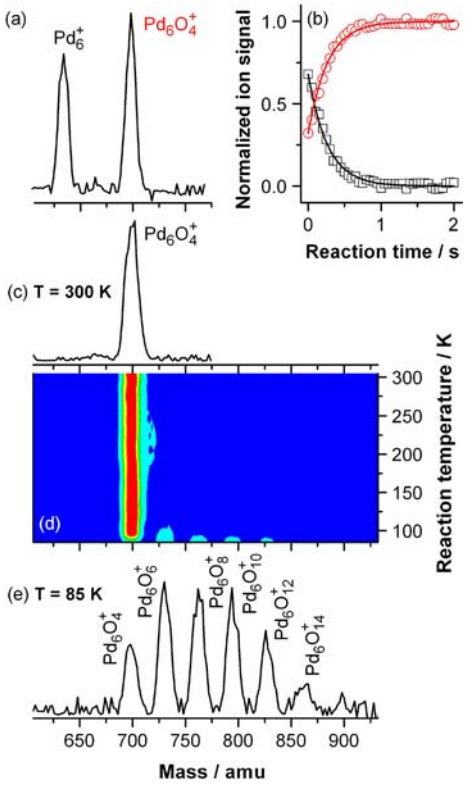

Figure 1. Reaction of $Pd_6O_4^+$ with molecular oxygen. (a) Ion mass distribution obtained at the highest investigated reaction temperature of 300 K under kinetically controlled reaction conditions ($p(O_2)$ = 0.01 Pa in 1 Pa of helium). (b) Corresponding kinetic data. (c) Steady-state equilibrium distribution detected at 300 K ($p(O_2)$ = 0.10 Pa; p(He) = 0.9 Pa). (d) 2D contour plot representation of the temperature-dependent product ion mass distributions recorded in steps of 10 K after trapping of $Pd_6O_4^+$ for 0.1 s in the presence of 0.10 Pa O_2 (p(He) = 0.9 Pa). The relative ion intensity is color coded from blue (0%) to red (100%). (c) Ion mass distribution obtained at the lowest investigated reaction temperature of 85 K.

interaction of Pd_6^+ with O_2, the corresponding kinetic data, that is, mass peak intensities as a function of the reaction time, were recorded; see Figure 1b. The lack of a signal for $Pd_6O_2^+$ and the exclusive formation of $Pd_6O_4^+$ identify the adsorption of a first O_2 molecule as the rate-determining reaction step, while the subsequent adsorption of the second O_2 molecule proceeds faster than the time resolution of the experiment.[19] Thus, the rate constant extracted from the kinetic data in Figure 1b corresponds to the formation of $Pd_6O_2^+$.

The reaction mechanism that fits best this kinetics is that of a straightforward association reaction:

$$Pd_6^+ + 2O_2 \rightarrow Pd_6O_2^+ + O_2 \rightarrow Pd_6O_4^+ \quad (4)$$

while an equilibrium reaction mechanism can be excluded on the basis of the kinetic data. The fitting procedure[15] yields a termolecular rate constant $k^{(3)}(Pd_6^+{-}O_2) = (7.0 \pm 3.9) \times 10^{-27}$ cm^6 s^{-1} for the adsorption of a first O_2 molecule. With respect to the adsorption of the second O_2 molecule, a lower limit of the rate constant can be estimated to amount to $k^{(3)}(Pd_6O_2^+{-}O_2) > 3.6 \times 10^{-25}$ cm^6 s^{-1}. These data already indicate the preferred formation and the potentially high stability of $Pd_6O_4^+$. Increasing the O_2 partial pressure by a factor of 10 (Figure 1c), while resulting in an increased reaction rate, maintains $Pd_6O_4^+$ as the sole product.

The particular stability of $Pd_6O_4^+$ is further supported experimentally by reactivity studies of Pd_7^+ with O_2 (not shown here), which result in the absence of any signals corresponding to the heptamer palladium cluster. Instead, one finds fragmentation into $Pd_6O_4^+$. The preferred formation and enhanced stability of $Pd_6O_4^+$ during the oxidation of Pd_6^+ and Pd_7^+ appear to be unique, as no comparable enhanced intensity and stability of a "tetroxide" cluster have been observed for oxidized clusters of the homologous elements nickel and platinum.[26] However, the interaction of NO with the rhodium hexamer Rh_6^+ has been reported to result in two N_2 molecules and the stable tetroxide cluster $Rh_6O_4^+$, which cannot dissociate further NO molecules.[27]

Cooling the ion trap also does not lead to additional oxidation products over a wide temperature range. Figure 1d shows a 2D contour plot representation of the temperature-dependent mass spectra. The tetroxide hexamer, $Pd_6O_4^+$, is found as the only reaction product between 100 and 300 K, and further multiple O_2 adsorption only occurs at temperatures as low as 85 K yielding $Pd_6O_x^+$ (x = 6, 8, 10, 12, 14); see the corresponding mass spectrum in Figure 1e. As indeed has been predicted by our first−principles DFT calculations (see below), in addition to the self-limiting oxidation of Pd_6^+ that yields exclusively an oxidation resistant tetroxide cluster $Pd_6O_4^+$, a second oxygen adsorption regime occurs at cryogenic temperatures, where a weakly bound molecularly adsorbed species is condensing on the cluster, rapidly desorbing at T > 100 K. Indications for the similar occurrence of two oxygen phases of "tetroxide" and molecularly physisorbed O_2 (at cryogenic temperatures) have also been observed for the smaller palladium clusters Pd_x^+, x = 3−5; however, this oxidation behavior is most striking for Pd_6^+.

To gain insight into the nature of the oxygen−palladium interaction and the geometry of the bare and oxidized clusters, as well as to understand the stability and the oxidation resistance of $Pd_6O_4^+$, first-principles DFT calculations have been performed.[20] Figure 2 (top row) displays the oxidation products of Pd_6^+. The first two oxygen molecules adsorb strongly in an activated molecular configuration in which each O_2 molecule bridges between neighboring Pd atoms (in the molecularly adsorbed state, the O−O bond length d(O−O) = 1.35 Å, as compared to 1.25 Å in the gas phase, signifying an activated superoxo state). This enables the facile dissociation of these activated molecules and the formation of an oxidized cluster with each oxygen bonded to three neighboring Pd atoms in $Pd_6O_4^+$ (Figure 2, middle of top row). This oxide cluster thus contains only strongly bound (chemisorbed) atomic oxygen, underlying its overall stability and resistance to further oxidation.

Indeed, interaction of $Pd_6O_4^+$ with a third oxygen molecule results in a weak molecularly adsorbed state, $Pd_6O_4^+(O_2)$, with the adsorbed molecule being nonactivated having d(O−O) = 1.26 Å and an adsorption energy of only δE = 0.33 eV. This value is significantly lower than the binding (δE = 4.63 eV) of the dissociatively adsorbed second molecule in $Pd_6O_4^+$ (see Figure 2). Hence, the observed oxidation resistance of $Pd_6O_4^+$ appears to originate from the inability of the Pd atoms of the cluster to bind strongly to more than two oxygen atoms; that is, binding to a double-oxygen-coordinated Pd atom results in a weakly adsorbed molecular state. Additionally, dissociation of adsorbed molecules above the self-limiting number is inhibited due to site-blocking by the already-adsorbed oxygen atoms.

dx.doi.org/10.1021/ja308189w | J. Am. Chem. Soc. 2012, 134, 20654−20659

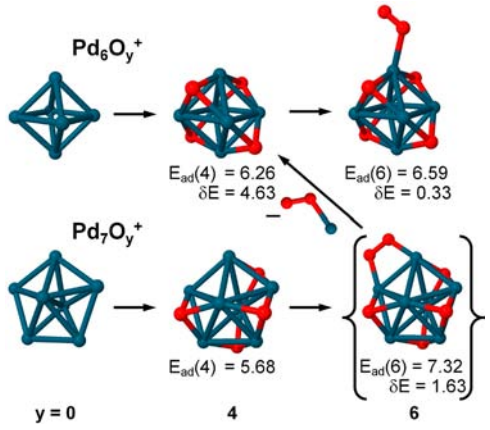

Figure 2. Ground-state atomic structures of $Pd_6O_y^+$ (top row) and $Pd_7O_y^+$ (bottom row) for y = 0, 4, 6. The structure in curly brackets depicts a transient intermediate (nonobservable). Next to each structure we give the total adsorption energy, relative to the bare cluster and free (y/2) O_2 molecules ($E_{ad}(y)$), and below it we give the adsorption energy of the last-added oxygen molecule (δE). The spin multiplicities of the lowest energy isomers of the clusters are as follows: Pd_6^+ s = 1.5 (3 unpaired electrons), spin multiplicity $S = 2s + 1 = 4$; $Pd_6O_4^+$ s = 0.5, S = 2; Pd_7^+ s = 1.5, S = 4; $Pd_7O_4^+$ s = 1.5, S = 4. The Pd and O atoms are represented by blue and red spheres, respectively. The energies are given in units of electronvolts.

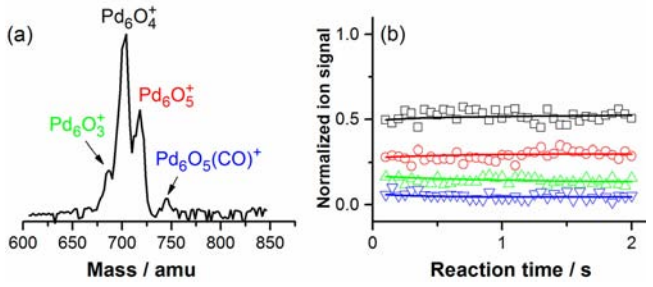

Figure 3. (a) Representative ion mass distribution obtained after a reaction time of 0.1 s and (b) corresponding kinetics of the reaction between Pd_6^+ and O_2/CO ($p(O_2)$ = 0.09 Pa; p(CO) = 0.01 Pa; p(He) = 0.9 Pa) recorded at 300 K. The open symbols represent the experimental data normalized to the total ion concentration in the ion trap. The solid lines are obtained by fitting the integrated rate equations of the proposed catalytic reaction cycle (see Scheme 1) to the experimental data.

The molecular level picture that emerges from these simulations reveals a chemisorbed atomic oxygen structure, $Pd_6O_4^+$, which resists further oxidation and limits the number of adsorbed oxygen at, and below, room temperature. Only at cryogenic temperatures can a second adsorption state, consisting of weakly physisorbed oxygen molecules, be stabilized on the cluster.

Furthermore, the theoretically determined fragmentation mechanism occurring during the reaction of Pd_7^+ with O_2 is shown in the bottom row of Figure 2. This mechanism confirms the experimental observation that only $Pd_6O_4^+$ results from the oxidation of Pd_7^+ (see discussion above). It may be described as a two-step process: in a first step, adsorption (with δE = 1.63 eV) of O_2 onto $Pd_7O_4^+$ results in formation of a transient (nonobservable) intermediate $Pd_7O_6^+$ (see configuration in curly brackets in Figure 2), and in a subsequent step, a PdO_2 molecule evaporates from the $Pd_7O_6^+$ intermediate; the overall two-step process entails an energy of 0.45 eV.

3.2. CO Oxidation. In a second gas-phase experiment, oxidation conditions similar to those in Figure 1c were established, and, in addition, a small partial pressure of carbon monoxide ($p(O_2)/p$(CO) = 9) was admitted to the ion trap at room temperature. The resulting ion mass distribution measured after 0.1 s reaction time is shown in Figure 3a. In addition to the previously detected single oxidation product $Pd_6O_4^+$, further mass peaks are observed, and they can be assigned to $Pd_6O_3^+$, $Pd_6O_5^+$, and $Pd_6O_5(CO)^+$. This indicates that a reaction with CO occurs, which, most interestingly, leads to the loss of oxygen atoms (or more likely, of course, the formation of CO_2) as apparent from the detection of clusters containing an odd number of O atoms. Yet, $Pd_6O_4^+$ still represents the most abundant product ion.

The corresponding kinetic data (Figure 3b) show a rapid saturation of all products (faster than the time resolution of the experiment) under the applied experimental conditions (steady state). Such kinetic data can be explained either by an equilibrium reaction mechanism with all products being connected by forward and backward reaction steps or by a catalytic reaction cycle. Because of the observation of the products $Pd_6O_3^+$, $Pd_6O_5^+$, and $Pd_6O_5(CO)^+$ containing an odd number of oxygen atoms, which only occur in the presence of CO, and due to the fact that there is no source of atomic oxygen present in the ion trap, an equilibrium reaction mechanism can be excluded. Hence, the products that are detected with both O_2 and CO in the ion trap must be formed as part of a catalytic reaction cycle.

The dominance of the oxidation product $Pd_6O_4^+$ at all reaction times and the lack of products containing only CO lead us to conclude that the reaction with two oxygen molecules and the formation of $Pd_6O_4^+$ represent the first reaction steps. This is corroborated by the excess of O_2 in the ion trap. Because $Pd_6O_4^+$ was found to be oxidation resistant at room temperature, the product $Pd_6O_5^+$ cannot result from the reaction of O_2 with $Pd_6O_4^+$. Instead, the subsequent reaction step must involve the reaction with CO leading to the formation of $Pd_6O_3^+$, most likely under the production and elimination of CO_2. $Pd_6O_3^+$ can then adsorb a further O_2 molecule yielding $Pd_6O_5^+$. The formation of this product is in agreement with concurrent oxidation studies of preoxidized Pd_6O^+ resulting in the sole oxidation product $Pd_6O_5^+$. The next reaction step must then describe the reaction of $Pd_6O_5^+$ with CO yielding $Pd_6O_5CO^+$, which represents a precursor for formation and elimination of a second CO_2 molecule leading to the reformation of $Pd_6O_4^+$. The following reaction equations describe this mechanism (see also Scheme 1):

$$Pd_6O_4^+ + CO \rightarrow Pd_6O_3^+ + CO_2, \quad k_1 \tag{5a}$$

$$Pd_6O_3^+ + O_2 \rightarrow Pd_6O_5^+, \quad k_2 \tag{5b}$$

$$Pd_6O_5^+ + CO \rightarrow Pd_6O_5CO^+, \quad k_3 \tag{5c}$$

$$Pd_6O_5CO^+ \rightarrow Pd_6O_4^+ + CO_2, \quad k_4 \tag{5d}$$

The good fit between the experimental data and the integrated rate equations of the above microkinetic model is shown (solid lines) in Figure 3b.

Because of the fact that the product concentrations presented in Figure 3b do not exhibit an initial decay or growth, respectively (rapid saturation), it is not possible to determine absolute pseudofirst-order rate constants for the reaction steps

dx.doi.org/10.1021/ja308189w | J. Am. Chem. Soc. 2012, 134, 20654−20659

Scheme 1. Proposed Catalytic Reaction Cycle Resulting from the Theoretically Determined Reaction Pathways, Which Also Represents the Best Fit of the Experimental Reaction Kinetic Data

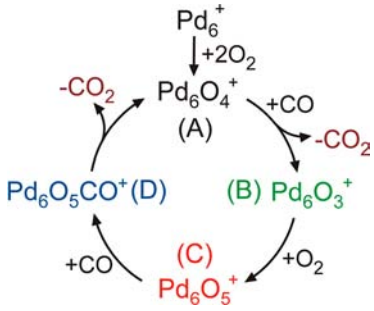

of the microkinetic model. Only a lower limit for k_1–k_4 of eq 5 can be estimated from the time resolution of the experiment ($k_{1-4} > 100\ s^{-1}$). Nevertheless, the rather small intensity of the intermediates $Pd_6O_3^+$ and $Pd_6O_5CO^+$ in Figure 3a suggests that the reaction steps 5b and 5d are still considerably faster than the reaction steps 5a and 5c. This is confirmed by the relative magnitudes of k_2 and k_4 with respect to k_1 and k_3, which depend, however, also on the CO and O_2 partial pressures.

Theoretically predicted reaction pathways describing the catalytic CO oxidation on the palladium tetroxide $Pd_6O_4^+$ are depicted in Figure 4 (see the Supporting Information for corresponding values of energies and distances), and the corresponding catalytic cycle is shown in Scheme 1. The solid lines in Figure 4 represent reaction mechanisms following a Langmuir–Hinshelwood (LH) reaction mechanism where reaction occurs through interaction of adsorbed molecules and atoms. All three shown LH mechanisms share the first part of the reaction mechanism including the barrier-free adsorption of a first CO molecule on $Pd_6O_4^+$ (configuration A) yielding $Pd_6O_4CO^+$ (E(CO) = 1.27 eV), the activated reaction of the adsorbed CO with an oxygen atom of the palladium tetroxide (activation barrier E_b = 1.22 eV), the elimination of the formed CO_2 molecule yielding $Pd_6O_3^+$ (configuration B, $E(CO_2)$ = 0.35 eV), and the subsequent adsorption of an oxygen molecule resulting in $Pd_6O_5^+$ (configuration C, $E(O_2)$ = 1.99 eV, d(O–O) = 1.38 Å). One possible reaction pathway (depicted by a dark green line) describes an activated dissociation of the adsorbed oxygen molecule involving an activation barrier of E_b = 0.76 eV and resulting in configuration C′ (d(O–O) = 2.8 Å). This oxide then adsorbs a second CO molecule barrier-free (E(CO) = 1.56 eV) yielding the experimentally observed complex $Pd_6O_5CO^+$ (configuration D). The catalytic cycle is closed by reformation of $Pd_6O_4^+$ and CO_2 involving an activation barrier of E_b = 0.81 eV.

An alternative pathway, where the (C) → (D) transition is barrierless, is marked by a light green solid line. This pathway proceeds via barrier-free formation of configuration D′ (E(CO) = 1.56 eV) and the activated formation of $Pd_6O_4^+$ (A) + CO_2, involving a barrier of 0.98 eV. A third alternative LH pathway (depicted in blue) proceeds via the activated formation of an intermediate (D″, E_b = 1.23 eV) containing a partially negatively charged (0.7e) CO_3 unit as well as the activated formation of CO_2 on the cluster (E_b = 1.34 eV).

The dashed lines in Figure 4 represent an alternative reaction pathway following an Eley–Rideal (ER) reaction mechanism where reaction occurs between an impinging gas-phase molecule and an adsorbed species. According to such an ER reaction mechanism, the interaction of $Pd_6O_4^+$ (configuration A) and CO leads to formation and elimination of a first CO_2 molecule via a small activation barrier of E_b = 0.55 eV resulting in $Pd_6O_3^+$ (B). This oxide adsorbs a second CO molecule (configuration C) and undergoes structural rearrangement yielding configuration C′ as already observed in the LH mechanism (dark green line). The subsequent adsorption of a second CO molecule and formation/liberation of CO_2 is barrier free. Furthermore, both reaction mechanism, the LH and ER reaction pathways, are modified by the Mars–van Krevelen[11] process of oxide formation prior to reaction with CO.

These calculated pathways and the catalytic cycle demonstrate the occurrence of effective CO oxidation by molecular

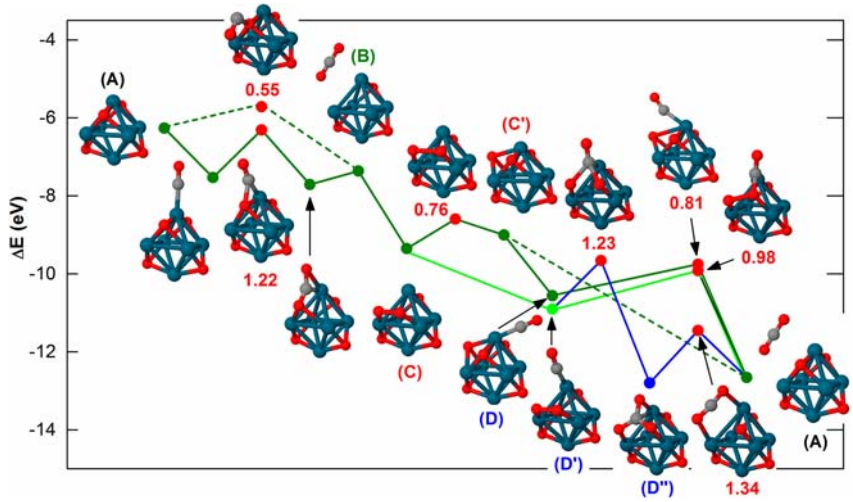

Figure 4. Calculated reaction pathways for the $Pd_6O_4^+$-catalyzed oxidation of CO. The reactive species, which were detected in the measured ion distribution (Figure 3a), are identified as: (A) $Pd_6O_4^+$, (B) $Pd_6O_3^+$, (C) $Pd_6O_5^+$, and (D) $Pd_6O_5CO^+$. Langmuir–Hinshelwood (LH) mechanisms (with both reactants adsorbed on the catalyst) are given by solid lines. Dashed lines correspond to Eley–Rideal (ER) mechanisms (one reactant adsorbed and the other impinging from the gas phase). Both mechanisms are modified by the Mars–van Krevelen[11] process of oxide formation prior to reaction with CO. The transition states (TS) are denoted by red dots, and the associated TS barrier energies (E_b) are given (in red) next to the TS configurations in electronvolts. Pd, O, and C atoms are represented by blue, red, and gray spheres, respectively.

dx.doi.org/10.1021/ja308189w | J. Am. Chem. Soc. 2012, 134, 20654–20659

oxygen, catalyzed, at room temperature, by palladium hexamer clusters. However, it is clear that Pd_6^+ itself is not part of the catalytic reaction cycle. Instead, the nano-oxide cluster $Pd_6O_4^+$ is identified as the catalytically active species (see Scheme 1). Interestingly, this is in contrast to previous CO oxidation experiments with platinum and gold clusters, where the bare metal clusters $Pt_n^{\pm}$ and Au_n^-, respectively, are part of the catalytic cycle.[28] The kinetic scheme (mechanism 5) used in fitting the experimental kinetic data (Figure 3b) is consistent with all of these predicted pathways as well as the resulting catalytic reaction cycle, while a cycle including Pd_6^+ does not fit the experimental data.

4. CONCLUSION

The nano-oxide cluster $Pd_6O_4^+$ was identified to be the key intermediate in the catalytic combustion of CO initiated by the oxidation of Pd_6^+ with molecular oxygen. $Pd_6O_4^+$ contains only dissociated oxygen with each O atom bound to three Pd atoms. Although $Pd_6O_4^+$ appears to be resistant to further oxidation with O_2, the chemisorbed atomic oxygen species represent the active oxygen phase for the efficient room temperature catalytic conversion of CO to CO_2. These gas-phase results provide information that may be utilized in the design of prospective new nano-oxide-based catalytic materials for low temperature oxidation catalysis.

■ ASSOCIATED CONTENT

Supporting Information

Details of the geometric data and energies of the reaction pathway. This material is available free of charge via the Internet at http://pubs.acs.org.

■ AUTHOR INFORMATION

Corresponding Author

thorsten.bernhardt@uni-ulm.de; uzi.landman@physics.gatech.edu

Notes

The authors declare no competing financial interest.

■ ACKNOWLEDGMENTS

We gratefully acknowledge financial support by the Deutsche Forschungsgemeinschaft. In particular, S.M.L. is grateful to the European Social Fund Baden-Württemberg for a Margarete von Wrangell fellowship. The work of U.L. and R.N.B. at the Georgia Institute of Technology was supported by a grant from the US AFOSR. Calculations were performed at the Georgia Institute of Technology Center for Computational Materials Science.

■ REFERENCES

(1) Ertl, G., Knözinger, H., Weitkamp, J., Eds. *Handbook of Heterogeneous Catalysis*; Wiley-VCH: Weinheim, 1997; Vol. *4*.

(2) Cuenya, B. R. *Thin Solid Films* **2010**, *518*, 3127−3150.

(3) (a) Gandhi, H. S.; Graham, G. W.; McCabe, R. W. *J. Catal.* **2003**, *216*, 433−442. (b) Centi, G.; Ciambelli, P.; Perathoner, S.; Russo, P. *Catal. Today* **2002**, *75*, 3−15.

(4) (a) Engel, T.; Ertl, G. *J. Chem. Phys.* **1978**, *69*, 1267−1281. (b) Conrad, H.; Ertl, G.; Küppers, J. *Surf. Sci.* **1978**, *76*, 323−342.

(5) (a) Meusel, I.; Hoffmann, J.; Hartmann, J.; Heemeier, M.; Bäumer, M.; Libuda, J.; Freund, H.-J. *Catal. Lett.* **2001**, *71*, 5−13. (b) Penner, S.; Bera, P.; Pedersen, S.; Ngo, L. T.; Harris, J. J. W.; Campbell, C. T. *J. Phys. Chem. B* **2006**, *110*, 24577−24584. (c) Shaikhutdinov, S.; Heemeier, M.; Hoffmann, J.; Meusel, I.; Richter, B.; Bäumer, M.; Kuhlenbeck, H.; Libuda, J.; Freund, H.-J.; Oldman, R.; Jackson, S. D.; Konvicka, C.; Schmid, M.; Varga, P. *Surf. Sci.* **2002**, *501*, 270−281. (d) Schalow, T.; Brandt, B.; Starr, D. E.; Laurin, M.; Shaikhutdinov, S. K.; Schauermann, S.; Libuda, J.; Freund, H.-J. *Angew. Chem., Int. Ed.* **2006**, *45*, 3693−3697.

(6) Schalow, T.; Laurin, M.; Brandt, B.; Schauermann, S.; Guimond, S.; Kuhlenbeck, H.; Starr, D. E.; Shaikhutdinov, S. K.; Libuda, J.; Freund, H.-J. *Angew. Chem., Int. Ed.* **2005**, *44*, 7601−7605.

(7) Gabasch, H.; Knop-Gericke, A.; Schlögl, R.; Borasio, M.; Weilach, C.; Rupprechter, G.; Penner, S.; Jenewein, B.; Hayek, K.; Klötzer, B. *Phys. Chem. Chem. Phys.* **2007**, *9*, 533−540.

(8) Huber, B.; Koskinen, P.; Häkkinen, H.; Moseler, M. *Nat. Mater.* **2006**, *5*, 44−47.

(9) Yoon, B.; Landman, U.; Habibpour, V.; Harding, C.; Kunz, S.; Heiz, U.; Moseler, M.; Walter, M. *J. Phys. Chem. C* **2012**, *116*, 9594−9607.

(10) Moseler, M.; Walter, M.; Yoon, B.; Landman, U.; Habibpour, V.; Harding, C.; Kunz, S.; Heiz, U. *J. Am. Chem. Soc.* **2012**, *134*, 7690−7699.

(11) (a) Mars, P.; van Krevelen, D. W. *Chem. Eng. Sci.* **1954**, *3*, 41−59. (b) Mars, P.; Maessen, J. G. H. *Proceedings of the Third ICC*; North-Holland: Amsterdam, 1954; Vol. *1*, p 39.

(12) Reber, A. C.; Khanna, S. N.; Tyo, E. C.; Harmon, C. L.; Castleman, A. W., Jr. *J. Chem. Phys.* **2011**, *135*, 234303.

(13) Lang, S. M.; Schnabel, T.; Bernhardt, T. M. *Phys. Chem. Chem. Phys.* **2012**, *14*, 9364−9370.

(14) Kalita, B.; Deka, R. C. *J. Am. Chem. Soc.* **2009**, *131*, 13252−13254.

(15) Bernhardt, T. M. *Int. J. Mass Spectrom.* **2005**, *243*, 1−29.

(16) Keller, R.; Nöhmeier, F.; Spädtke, P.; Schönenberg, M. H. *Vacuum* **1984**, *34*, 31−35.

(17) Schuhmacher, E. *DETMECH - Chemical Reaction Kinetics Software*; University of Bern, Chemistry Department: Bern, 2003.

(18) (a) Steinfeld, J. I.; Francisco, J. S.; Hase, W. L. *Chemical Kinetics and Dynamics*, 2nd ed.; Prentice Hall: Upper Saddle River, 1999. (b) Laidler, K. J. *Chemical Kinetics*; Harper Collins: New York, 1987.

(19) Bernhardt, T. M.; Hagen, J.; Lang, S. M.; Popolan, D. M.; Socaciu-Siebert, L. D.; Wöste, L. *J. Phys. Chem. A* **2009**, *113*, 2724−2733.

(20) Barnett, R. N.; Landman, U. *Phys. Rev. B* **1993**, *48*, 2081−2097.

(21) Troullier, N.; Martins, J. L. *Phys. Rev. B* **1991**, *43*, 1993−2006.

(22) Perdew, J. P.; Burke, K.; Ernzerhof, M. *Phys. Rev. Lett.* **1996**, *77*, 3865−3868.

(23) (a) Moseler, M.; Häkkinen, H.; Barnett, R. N.; Landman, U. *Phys. Rev. Lett.* **2001**, *86*, 2545−2548. (b) Moseler, M.; Häkkinen, H.; Landman, U. *Phys. Rev. Lett.* **2002**, *89*, 176103.

(24) Bernhardt, T. M.; Heiz, U.; Landman, U. Chemical and Catalytic Properties of Size-Selected Free and Supported Clusters. In *Nanocatalysis*; Heiz, U., Landman, U., Eds.; Springer-Verlag: Berlin, Heidelberg, 2007; pp 1−191.

(25) Hintz, P. A.; Ervin, K. M. *J. Chem. Phys.* **1995**, *103*, 7897−7906.

(26) (a) Vann, W. D.; Bell, R. C.; Castleman, A. W., Jr. *J. Phys. Chem. A* **1999**, *103*, 10846−10850. (b) Koszinowski, K.; Schröder, D.; Schwarz, H. *J. Phys. Chem. A* **2003**, *107*, 4999−5006.

(27) Ford, M. S.; Anderson, M. L.; Barrow, M. P.; Woodruff, D. P.; Drewello, T.; Derrick, P. J.; Mackenzie, S. R. *Phys. Chem. Chem. Phys.* **2005**, *7*, 975−980.

(28) (a) Shi, Y.; Ervin, K. M. *J. Chem. Phys.* **1998**, *108*, 1757−1760. (b) Balaj, O. P.; Balteanu, I.; Roßteuscher, T. T. J.; Beyer, M. K.; Bondybey, V. E. *Angew. Chem., Int. Ed.* **2004**, *43*, 6519−6522. (c) Socaciu, L. D.; Hagen, J.; Bernhardt, T. M.; Wöste, L.; Heiz, U.; Häkkinen, H.; Landman, U. *J. Am. Chem. Soc.* **2003**, *125*, 10437−10445. (d) Wallace, W. T.; Whetten, R. L. *J. Am. Chem. Soc.* **2002**, *124*, 7499−7505.